Pramana – J. Phys. (2017) 88: 31
DOI 10.1007/s12043-016-1336-1

Lie group analysis of flow and heat transfer of non-Newtonian nanofluid over a stretching surface with convective boundary condition

AHMED A AFIFY[1,2,*] and MOHAMED ABD EL-AZIZ[1,3]

[1]Helwan University, Faculty of Science, Mathematics Department, P.O. Box 11795, Cairo, Egypt
[2]Department of Mathematics, Deanship of Educational Services, Qassim University, P.O. Box 6595, Buraidah: 51452 Saudi Arabia
[3]Department of Mathematics, Faculty of Science, King Khalid University, Abha 9004, Saudi Arabia
*Corresponding author. E-mail: afify65@yahoo.com

MS received 6 February 2015; revised 29 June 2016; accepted 29 July 2016; published online 9 January 2017

Abstract. The steady two-dimensional flow and heat transfer of a non-Newtonian power-law nanofluid over a stretching surface under convective boundary conditions and temperature-dependent fluid viscosity has been numerically investigated. The power-law rheology is adopted to describe non-Newtonian characteristics of the flow. Four different types of nanoparticles, namely copper (Cu), silver (Ag), alumina (Al_2O_3) and titanium oxide (TiO_2) are considered by using sodium alginate (SA) as the base non-Newtonian fluid. Lie symmetry group transformations are used to convert the boundary layer equations into non-linear ordinary differential equations. The transformed equations are solved numerically by using a shooting method with fourth-order Runge–Kutta integration scheme. The results show that the effect of viscosity on the heat transfer rate is remarkable only for relatively strong convective heating. Moreover, the skin friction coefficient and the rate of heat transfer increase with an increase in Biot number.

Keywords. Lie group analysis; boundary layer; nanofluid; non-Newtonian power-law fluid; variable viscosity; convective boundary conditions.

PACS Nos 44.20.+b; 65.80.−g; 02.20.−a; 47.50.−d

1. Introduction

The study of non-Newtonian fluid flow and heat transfer over a stretching surface has gained wide interest amongst researchers for the past two decades because of its industrial and engineering applications. In view of all these applications, Crane [1] initiated the analytical study of boundary layer flow due to a stretching sheet. Later on, many researchers [2–11] have effectively applied the Crane's model [1] for both Newtonian and non-Newtonian boundary layer flows.

Nanofluids are uniform and stable suspensions of metallic and/or non-metallic nanoparticles in a conventional heat transfer fluid such as water, glycerol–water mixture (Newtonian fluids) and dilute aqueous polymer solutions of sodium carboxymethyl cellulose (SCMC) and sodium alginate (SA) (non-Newtonian fluids). Applying nanotechnology to heat transfer, the new concept of 'nanofluid', introduced by Choi [12] has proposed to meet the new heat transfer challenges. Putra *et al* [13] studied free convection heat transfer of Al_2O_3–water and Cu–water nanofluids inside a horizontal cylinder heated from one end and cooled from the other. Many investigators have studied the various characteristics of fluid flow and heat transfer behaviour of nanofluids [14–20], and found that enhanced heat transfer coefficients were obtained with nanofluids.

The rheological behaviour of nanofluids has often been modelled using the power-law model with its two fitting parameters: the power-law index and the fluid viscosity. Kamali and Binesh [21] investigated the enhancement in heat transfer using carbon nanotube-based non-Newtonian nanofluids in a straight tube under constant wall heat flux condition. Recently, many experimental and numerical investigations [22–27] have been carried out to determine convective heat transfer characteristics of nanofluids using non-Newtonian fluid as the base fluid. Heat transfer under convective

boundary conditions plays a vital role in thermal energy storage, gas turbines, nuclear plants etc. In view of the above applications, Makinde and Aziz [28] investigated the boundary layer flow of a nanofluid past a stretching sheet under convective boundary condition. The analytical simulation of the problem of oblique stagnation point flow of a non-Newtonian fluid (Casson model) under convective boundary conditions is performed by Nadeem *et al* [29].

In all the above studies, the physical properties of the nanofluids were assumed to be constant. However, it is well known that the physical properties of the nanofluids may change with temperature. For heat transfer in fluids, heat generated by internal friction and the corresponding rise in the temperature affects the viscosity of the fluid, so that the fluid viscosity no longer is assumed to be constant. Abu-Nada [30] studied the effect of variable properties of Al_2O_3–water nanofluids on natural convection in an annular region. Vajravelu and Prasad [31] investigated the effects of variable fluid properties on the boundary layer flow and heat transfer of a nanofluid past a flat sheet. Recently, Afify and Bazid [32] analysed the boundary layer flow and transfer characteristics along a moving permeable surface immersed in nanofluids with temperature-dependent viscosity and viscous dissipation effects. To the best of our knowledge, the influences of convective boundary conditions and temperature-dependent fluid viscosity on flow and heat transfer characteristics of non-Newtonian power-law nanofluids over a non-linearly stretching surface have not been investigated. The results in our work may serve as a complement to the previous studies and provide useful information for engineering applications in medical arena as well as in electronics and transportations.

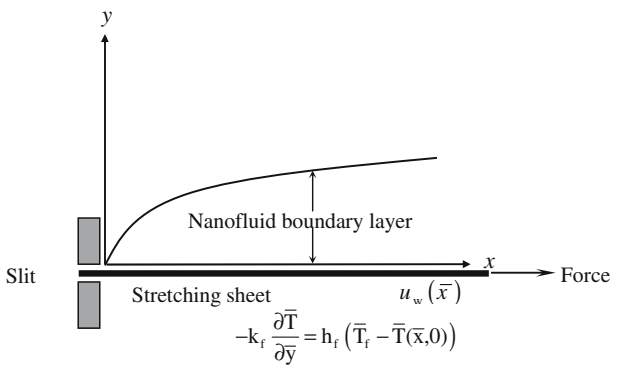

Figure 1. Physical model and coordinate system.

2. Formulation of the problem

We consider a steady, laminar boundary layer of a power-law non-Newtonian nanofluid past a stretching surface. The surface is stretching with the velocity $u_w(\bar{x})$ along the $\bar{x}$-direction while the $\bar{y}$-axis is taken normal to the surface, as shown in figure 1. The thermophysical nanofluid properties are assumed to be isotropic and constant, except for the fluid viscosity which is assumed to vary with temperature. The thermophysical properties of the nanofluid are given in table 1. The nanofluid is treated as a power-law non-Newtonian fluid under convective boundary conditions. The fluid is sodium alginate (SA) based nanofluid containing different types of nanoparticles: Copper (Cu), silver (Ag), alumina (Al_2O_3) and titania (TiO_2). The nanofluid is assumed to be incompressible and the flow is assumed to be laminar. It is also assumed that the bottom surface of the stretching surface is heated by convection from a hot fluid of temperature T_f which provides a heat transfer coefficient $h_f(\bar{x})$. Under the usual boundary layer approximation, the governing boundary layer equations are:

$$\frac{\partial \bar{u}}{\partial \bar{x}} + \frac{\partial \bar{v}}{\partial \bar{y}} = 0, \tag{1}$$

$$\bar{u}\frac{\partial \bar{u}}{\partial \bar{x}} + \bar{v}\frac{\partial \bar{u}}{\partial \bar{y}} = \frac{1}{\rho_{nf}}\frac{\partial \tau_{\bar{x}\bar{y}}}{\partial \bar{y}}, \tag{2}$$

$$\bar{u}\frac{\partial T}{\partial \bar{x}} + \bar{v}\frac{\partial T}{\partial \bar{y}} = \alpha_{nf}\frac{\partial^2 T}{\partial \bar{y}^2}. \tag{3}$$

The boundary conditions are given by

$$\begin{aligned} &\bar{y} = 0 : \bar{u} = \bar{u}_w(\bar{x}) = \left(\frac{\bar{x}}{L}\right)^{1/3} U_0, \quad \bar{v} = 0, \\ &-k_f\frac{\partial \bar{T}}{\partial \bar{y}} = h_f\left(\frac{\bar{x}}{L}\right)(\bar{T}_f - \bar{T}(\bar{x},0)), \\ &\bar{y} \to \infty : \bar{u} \to 0, \bar{T} \to T_\infty. \end{aligned} \tag{4}$$

Table 1. Thermophysical properties of fluid and nanoparticles.

	ρ (kg/m^2)	C_p (J/kg)	k (W/mK)
Sodium alginate (SA)	989	4175	0.6376
Copper (Cu)	8933	385	401
Silver (Ag)	10500	235	429
Alumina (Al_2O_3)	3970	765	40
Titanium oxide (TiO_2)	4250	686.2	8.9538

The power-law model is used for the non-Newtonian fluid, according to which the relationship between the shear stress and the strain rate is given as follows:

$$\tau_{\bar{x}\bar{y}} = -\mu_{\rm nf}\left(-\frac{\partial \bar{u}}{\partial \bar{y}}\right)^n. \tag{5}$$

When $n = 1$, the constitutive equation represents Newtonian fluid with the dynamic coefficient of viscosity $\mu_{\rm f}$. If $n \prec 1$ the fluid is said to be pseudoplastic (shear thinning fluids) and if $n \succ 1$ it is called dilatant (shear thickening fluids). Substituting eq. (5) into eq. (2) we get

$$\bar{u}\frac{\partial \bar{u}}{\partial \bar{x}} + \bar{v}\frac{\partial \bar{u}}{\partial \bar{y}} = -\frac{1}{\rho_{\rm nf}}\frac{\partial}{\partial \bar{y}}\left[\mu_{\rm nf}\left(-\frac{\partial \bar{u}}{\partial \bar{y}}\right)^n\right]. \tag{6}$$

The density, heat capacity and thermal diffusivity of the nanofluid are as follows [33]:

$$\rho_{\rm nf} = (1-\varphi)\rho_{\rm f} + \varphi\rho_{\rm s},$$
$$(\rho C_{\rm p})_{\rm nf} = (1-\varphi)(\rho C_{\rm p})_{\rm f} + \varphi(\rho C_{\rm p})_{\rm s},$$
$$\alpha_{\rm nf} = \frac{k_{\rm nf}}{(\rho C_{\rm p})_{\rm nf}}. \tag{7}$$

Wang *et al* [34] developed a model to predict the viscosity of nanofluid as follows:

$$\mu_{\rm nf} = (1 + 7.3\varphi + 123\varphi^2)\mu_{\rm f}. \tag{8}$$

The effective thermal conductivity of the nanofluid is determined using the Maxwell model [35] which is:

$$\frac{k_{\rm nf}}{k_{\rm f}} = \frac{(k_{\rm s}+2k_{\rm f}) - 2\varphi(k_{\rm f}-k_{\rm s})}{(k_{\rm s}+2k_{\rm f}) + \varphi(k_{\rm f}-k_{\rm s})}. \tag{9}$$

Here $k_{\rm f}$ is the thermal conductivity of the fluid, $k_{\rm s}$ is the thermal conductivity of the solid, φ is the volume fraction of the nanoparticle, $\rho_{\rm f}$ is the reference density of the fluid fraction, $\rho_{\rm s}$ is the reference density of the solid fraction, $C_{\rm p}$ is the specific heat, $\mu_{\rm f}$ is the cofficient of viscosity of the base fluid, u and v are the velocity components along the x- and the y-axes respectively.

It is worth mentioning that the viscosity of the base fluid sodium alginate (SA) is considered to vary with temperature. The temperature-dependent viscosity can be expressed as [36]

$$\mu_{\rm f} = \mu_\infty \exp[-\beta_0(\bar{T} - T_\infty)]. \tag{10}$$

In relation (10), $\beta = \beta_0(T_{\rm f} - T_\infty)$ is the viscosity parameter and T_∞ and μ_∞ are the constant values of temperature and coefficient of viscosity far away from the surface, respectively. In view of relations (7), (8) and (10), eqs (3) and (6) become

$$\bar{u}\frac{\partial \bar{T}}{\partial \bar{x}} + \bar{v}\frac{\partial \bar{T}}{\partial \bar{y}} = \frac{k_{\rm nf}}{(\rho C_{\rm p})_{\rm nf}}\frac{\partial^2 \bar{T}}{\partial \bar{y}^2} \tag{11}$$

$$\bar{u}\frac{\partial \bar{u}}{\partial \bar{x}} + \bar{v}\frac{\partial \bar{u}}{\partial \bar{y}} = -\frac{1}{(1-\varphi)\rho_{\rm f} + \varphi\rho_{\rm s}} \times \frac{\partial}{\partial \bar{y}}\left[(1 + 7.3\varphi + 123\varphi^2)\mu_\infty \times \exp[-\beta_0(\bar{T} - T_\infty)]\left(-\frac{\partial \bar{u}}{\partial \bar{y}}\right)^n\right]. \tag{12}$$

2.1 *Lie symmetry analysis*

Introducing the following dimensionless variables as [37–39]

$$x = \frac{\bar{x}}{L}, \quad y = \frac{\bar{y}}{L}\left(\frac{\rho_{\rm f}U_0^{2-n}L^n}{\mu_\infty}\right)^{1/(n+1)}, \quad u = \frac{\bar{u}}{U_0},$$
$$v = \frac{\bar{v}}{U_0}\left(\frac{\rho_{\rm f}U_0^{2-n}L^n}{\mu_\infty}\right)^{1/(n+1)}, \quad \theta = \frac{\bar{T} - T_\infty}{T_{\rm f} - T_\infty}, \tag{13}$$

and also introducing stream function ψ defined as

$$u = \frac{\partial \psi}{\partial y} \quad \text{and} \quad v = -\frac{\partial \psi}{\partial x}. \tag{14}$$

In view of the relations (7)–(10), (13) and (14), continuity eq. (1) is satisfied. Also eqs (11) and (12) are transformed to

$$\Delta_1 = \frac{\partial \psi}{\partial y}\frac{\partial^2 \psi}{\partial x \partial y} - \frac{\partial \psi}{\partial x}\frac{\partial^2 \psi}{\partial y^2} - \left(\frac{(1 + 7.3\varphi + 123\varphi^2)\mathrm{e}^{-\beta\theta}}{(1 - \varphi + \varphi(\rho_{\rm s}/\rho_{\rm f}))} \cdot \left[n\left(-\frac{\partial^2 \psi}{\partial y^2}\right)^{n-1}\frac{\partial^3 \psi}{\partial y^3} + \beta\frac{\partial \theta}{\partial y}\left(-\frac{\partial^2 \psi}{\partial y^2}\right)^n\right]\right) = 0 \tag{15}$$

$$\Delta_2 \equiv \frac{\partial \psi}{\partial y}\frac{\partial \theta}{\partial x} - \frac{\partial \psi}{\partial x}\frac{\partial \theta}{\partial y} - \frac{k_{\rm nf}/k_{\rm f}}{\left[1 - \varphi + \varphi\frac{(\rho C_{\rm p})_{\rm s}}{(\rho C_{\rm p})_{\rm f}}\right]}\frac{1}{\mathrm{Pr}_\infty}\frac{\partial^2 \theta}{\partial y^2} = 0 \tag{16}$$

and the boundary conditions (4) take the form

$$y = 0\colon \frac{\partial \psi}{\partial y} = x^{1/3}, \quad -\frac{\partial \psi}{\partial x} = 0,$$
$$\frac{\partial \theta}{\partial y} = -h_{\rm f}(x)\,\frac{L}{k_{\rm f}}\left(\frac{U_0^{2-n}L^n}{\upsilon_\infty}\right)^{-1/(n+1)}(1-\theta)$$
$$y \to \infty\colon \frac{\partial \psi}{\partial y} = 0, \quad \theta = 0. \tag{17}$$

We introduce the following special form of Lie group transformations [40,41]:

$$\Gamma\colon \begin{cases} x^* = x\mathrm{e}^{\epsilon\alpha_1},\ y^* = y\mathrm{e}^{\epsilon\alpha_2},\ \psi^* = \psi\mathrm{e}^{\epsilon\alpha_3},\ h_{\rm f}^* = h_{\rm f}\mathrm{e}^{\epsilon\alpha_4}, \\ \theta^* = \theta\mathrm{e}^{\epsilon\alpha_5}. \end{cases} \tag{18}$$

Here, ϵ is the parameter of the group and α_i ($i = 1$, 2, ..., 5) are arbitrary real numbers whose interrelationship will be determined by our analysis. Equation (18) is considered as a point transformation which transforms the coordinates $(x,\ y,\ \psi,\ h_{\rm f},\ \theta)$ to $(x^*,\ y^*,\ \psi^*,\ h_{\rm f}^*,\ \theta^*)$. We now investigate the relationship among the exponents α_i ($i = 1, 2, ..., 5$) such that

$$\Delta_j\left(x^*, y^*, \psi^*, ..., \frac{\partial\psi^*}{\partial y^3}\right) = H_j\left(x, y, \psi, ..., \frac{\partial^3\psi}{\partial y^3}; \alpha\right) \times \Delta_j\left(x, y, \psi, ..., \frac{\partial\psi}{\partial y^3}\right), \quad j = 1, 2. \tag{19}$$

Equations (15) and (16) are invariant under the group of transformation Γ [42]. Using eq. (18), then eqs (15) and (16) become

$$\begin{aligned}\Delta_1 \equiv{}& \frac{\partial\psi^*}{\partial y^*}\frac{\partial^2\psi^*}{\partial x^*\partial y^*} - \frac{(1 + 7.3\varphi + 123\varphi^2)\mathrm{e}^{-\beta\theta^*}}{(1 - \varphi + \varphi(\rho_{\rm s}/\rho_{\rm f}))} \times \left[n\left(-\frac{\partial^2\psi^*}{\partial y^{*2}}\right)^{n-1}\frac{\partial^3\psi^*}{\partial y^{*3}} + \beta\frac{\partial\theta^*}{\partial y^*}\left(-\frac{\partial^2\psi^*}{\partial y^{*2}}\right)^n\right] \\ ={}& \mathrm{e}^{\epsilon(2\alpha_3 - 2\alpha_2 - \alpha_1)}\left(\frac{\partial\psi}{\partial y}\frac{\partial^2\psi}{\partial x\partial y} - \frac{\partial\psi}{\partial x}\frac{\partial^2\psi}{\partial y^2}\right) - \Bigg(\frac{(1 + 7.3\varphi + 123\varphi^2)\mathrm{e}^{-\beta\theta}}{(1 - \varphi + \varphi(\rho_{\rm s}/\rho_{\rm f}))} \cdot \Bigg[n\left(-\frac{\partial^2\psi}{\partial y^2}\right)^{n-1}\frac{\partial^3\psi}{\partial y^3}\mathrm{e}^{\epsilon(n\alpha_3 - \alpha_2(2n+1))} \\ &+ \beta\frac{\partial\theta}{\partial y}\left(-\frac{\partial^2\psi}{\partial y^2}\right)^n \mathrm{e}^{\epsilon((\alpha_5 - \alpha_2) + (\alpha_3 - 2\alpha_2)n)}\Bigg]\Bigg),\end{aligned} \tag{20}$$

$$\begin{aligned}\Delta_2 \equiv{}& \frac{\partial\psi^*}{\partial y^*}\frac{\partial\theta^*}{\partial x^*} - \frac{\partial\psi^*}{\partial x^*}\frac{\partial\theta^*}{\partial y^*} - \left[\frac{k_{\rm nf}/k_{\rm f}}{\left[1 - \varphi + \varphi[(\rho C_{\rm p})_{\rm s}/(\rho C_{\rm p})_{\rm f}]\right]}\frac{1}{\mathrm{Pr}_\infty}\right]\frac{\partial^2\theta^*}{\partial y^{*2}} \\ ={}& \mathrm{e}^{\epsilon(\alpha_5 + \alpha_3 - \alpha_2 - \alpha_1)}\left(\frac{\partial\psi}{\partial y}\frac{\partial\theta}{\partial x} - \frac{\partial\psi}{\partial x}\frac{\partial\theta}{\partial y}\right) - \mathrm{e}^{\epsilon(\alpha_5 - 2\alpha_2)} \times \left[\frac{k_{\rm nf}/k_{\rm f}}{\left[1 - \varphi + \varphi[(\rho C_{\rm p})_{\rm s}/(\rho C_{\rm p})_{\rm f}]\right]}\frac{1}{\mathrm{Pr}_\infty}\right]\frac{\partial^2\theta}{\partial y^2}.\end{aligned} \tag{21}$$

The system remains invariant under the group transformation Γ, and the following relations among the parameters are deduced:

$$\begin{aligned}2\alpha_3 - 2\alpha_2 - \alpha_1 &= n\alpha_3 - \alpha_2(2n + 1) \\ &= \alpha_5 - \alpha_2 + (\alpha_3 - 2\alpha_2)n; \\ \alpha_5 + \alpha_3 - \alpha_2 - \alpha_1 &= \alpha_5 - 2\alpha_2.\end{aligned} \tag{22}$$

The boundary conditions will be invariant under Γ if the following equations hold:

$$\begin{aligned}&\alpha_3 - \alpha_2 = \frac{1}{3}\alpha_1, \\ &\alpha_5 - \alpha_2 = \alpha_4 = \alpha_4 + \alpha_5.\end{aligned} \tag{23}$$

Solving eqs (22) and (23) gives

$$\alpha_2 = \frac{1}{3}\alpha_1, \quad \alpha_3 = \frac{2}{3}\alpha_1, \quad \alpha_4 = -\frac{1}{3}\alpha_1, \quad \alpha_5 = 0. \tag{24}$$

With these relationships among α's, the set of transformations Γ, reduces to:

$$\Gamma: \begin{cases} x^* = x\mathrm{e}^{\epsilon\alpha_1},\ y^* = \mathrm{e}^{\epsilon(\alpha_1/3)}y,\ \psi^* = \psi\mathrm{e}^{\epsilon(2\alpha_1/3)},\ \theta^* = \theta, \\ h_{\rm f}^* = h_{\rm f}\,\mathrm{e}^{-\epsilon(\alpha_1/3)}. \end{cases} \tag{25}$$

Expanding eq. (25) by Taylor's series in powers of ϵ and keeping terms up to the order ϵ, we get the characteristic equations:

$$\frac{\mathrm{d}x}{x} = \frac{3\mathrm{d}y}{y} = \frac{3\mathrm{d}\psi}{2\psi} = \frac{\mathrm{d}\theta}{0} = \frac{-3\mathrm{d}h_{\rm f}}{h_{\rm f}}. \tag{26}$$

2.2 *Similarity equations*

Solving the characteristic equations (21) we obtain,

$$\begin{aligned}&\eta = yx^{-1/3}, \quad \psi = x^{2/3}f(\eta), \\ &\theta = \theta(\eta), \quad h_{\rm f} = (h_{\rm f})_0 x^{-1/3}.\end{aligned} \tag{27}$$

Substitution of eq. (27) into eqs (15) and (16) leads to the following similarity equations:

$$n(-f'')^{n-1}f''' + \beta\theta'(-f'')^n + \frac{(1 - \varphi + \varphi(\rho_{\rm s}/\rho_{\rm f}))\,\mathrm{e}^{\beta\theta}}{(1 + 7.3\varphi + 123\varphi^2)}\left(\frac{2}{3}ff'' - \frac{1}{3}f'^2\right) = 0, \tag{28}$$

$$\left(\frac{k_{\rm nf}}{k_{\rm f}}\frac{1}{\mathrm{Pr}_\infty}\right)\theta'' + \frac{2}{3}\left((1 - \varphi) + \varphi\frac{(\rho C_{\rm p})_{\rm s}}{(\rho C_{\rm p})_{\rm f}}\right)f\theta' = 0, \tag{29}$$

with the boundary conditions

$$\begin{aligned}&f' = 1, \quad f = 0, \quad \theta' = -\mathrm{Bi}(1 - \theta) \quad \text{at } \eta = 0, \\ &f' \longrightarrow 0, \quad \theta \longrightarrow 0 \quad \text{as } \eta \longrightarrow \infty.\end{aligned} \tag{30}$$

The assumption of constant Prandtl number inside the boundary layer when the viscosity is temperature dependent, leads to unrealistic results [43,44]. Following Rahman *et al* [45] the Prandtl number is defined as

$$\mathrm{Pr} = \underset{\infty}{\mathrm{Pr}}\, \mathrm{e}^{-2\beta\theta/(n+1)}. \tag{31}$$

For $\beta = 0$, therefore, the variable Prandtl number Pr is equal to the ambient Prandl number Pr_∞ and it is independent of the values of β. Substituting eq. (31) into eq. (29), we obtain

$$\left(\frac{k_{\mathrm{nf}}}{k_{\mathrm{f}}}\right)\theta'' + \left[\frac{2}{3}\left((1-\varphi)+\varphi\frac{(\rho C_{\mathrm{p}})_{\mathrm{s}}}{(\rho C_{\mathrm{p}})_{\mathrm{f}}}\right) f\theta'\right] \times \mathrm{Pr}\,\mathrm{e}^{2\beta\theta/(n+1)} = 0, \tag{32}$$

where the prime denotes differentiation with respect to η, f is the similarity function, θ is the dimensionless temperature,

$$\underset{\infty}{\mathrm{Pr}} = \frac{(\rho C_{\mathrm{p}})_{\mathrm{f}}}{k_{\mathrm{f}}}\left(\left(\frac{\mu_\infty}{\rho_{\mathrm{f}}}\right)^2 U_0^{3(n-1)} L^{1-n}\right)^{1/(n+1)}$$

is the ambient Prandtl number,

$$\mathrm{Pr} = \frac{(\rho C_{\mathrm{p}})_{\mathrm{f}}}{k_{\mathrm{f}}}\left(\left(\frac{\mu_{\mathrm{f}}}{\rho_{\mathrm{f}}}\right)^2 U_0^{3(n-1)} L^{1-n}\right)^{1/(n+1)}$$

is the variable Prandtl number,

$$\beta = \beta_0\,(T_{\mathrm{f}} - T_\infty)$$

is the viscosity variation parameter,

$$\mathrm{Bi} = (h_{\mathrm{f}})_0\,\frac{L}{k_{\mathrm{f}}}\left(\frac{U_0^{(2-n)} L^n}{\nu_\infty}\right)^{-1/(n+1)}$$

is the Biot number, $(h_{\mathrm{f}})_0$ is the heat transfer coefficient, n is the power-law index and L is the characteristic length. We also note that when $\varphi = \beta = 0$ in the absence of energy equation, eq. (28) reduces to those of Andersson and Kumaran [46] with $m = 1/3$ and Cortell [47,48] in the case of Newtonian fluid. The quantities of physical interest in this problem are skin friction coefficient and local Nusselt number, which are defined by

$$\mathrm{Re}_x^{1/(n+1)} C_{\mathrm{f}} = 2(1+7.3\varphi+123\varphi^2)\mathrm{e}^{-\beta\theta}(-f''(0))^n, \tag{33}$$

$$\mathrm{Re}_x^{1/(n+1)}\mathrm{Nu}_x = -\frac{k_{\mathrm{nf}}}{k_{\mathrm{f}}}\theta'(0), \tag{34}$$

where $\mathrm{Re}_x = x^n u_w^{2-n}/\nu_\infty$ is the local Reynolds number.

3. Numerical procedure

The nonlinear differential equations (28) and (32) along with the boundary conditions (30) form a two-point boundary value problem (BVP) and are solved using the shooting method, by converting into an initial value problem (IVP). In this method, the system of eqs (28) and (32) is converted into the set of the following first-order system:

$$f' = p, \quad p' = q,$$

$$q' = \frac{-(-q)^{1-n}}{n}\left[\beta z\,(-q)^n + \frac{(1-\varphi+\varphi(\rho_{\mathrm{s}}/\rho_{\mathrm{f}}))\,\mathrm{e}^{\beta\theta}}{(1+7.3\varphi+123\varphi^2)} \times \left(\frac{2}{3}fq - \frac{1}{3}p^2\right)\right], \tag{35}$$

$$\theta' = z,$$

$$z' = -(k_{\mathrm{f}}/k_{\mathrm{nf}}) \times \left[\frac{2}{3}\left(1-\varphi+\frac{(\rho C_{\mathrm{p}})_{\mathrm{s}}}{(\rho C_{\mathrm{p}})_{\mathrm{f}}}\varphi\right) fz\right]\mathrm{Pr}\,\mathrm{e}^{2\beta\theta/(n+1)} \tag{36}$$

with the initial conditions,

$$p(0) = 1, \quad f(0) = 0, \quad \theta'(0) = -\mathrm{Bi}(1-\theta(0)). \tag{37}$$

To solve eqs (35) and (36) with (37) as an IVP we must need the values for $q(0)$, i.e. $f''(0)$ and $\theta(0)$ but no such values are given. The initial guess values for $f''(0)$ and $\theta(0)$ are chosen and the fourth-order Runge–Kutta integration scheme is applied to obtain the solutions of (35) and (36) satisfying the initial conditions (37). Then we compare the calculated values $f'(\eta)$ and $\theta(\eta)$ at $\eta_\infty = 15$ with the given boundary conditions $f'(\eta_\infty) = 0$ and $\theta(\eta_\infty) = 0$ and adjust the values of $f''(0)$ and $\theta'(0)$, using 'secant method' to give better approximation for the solution. The step-size is taken as $\Delta\eta = 0.01$. The process is repeated until we get the results correct up to the desired accuracy of 10^{-5} level, which fulfills the convergence criterion.

4. Results and discussion

The set of nonlinear ordinary differential equations of (28) and (32) subject to the boundary conditions (30) are solved numerically by using the shooting method with fourth-order Runge–Kutta integration scheme. The local skin friction coefficient $\mathrm{Re}_x^{1/(n+1)} C_{\mathrm{f}}$ and the local Nusselt number $\mathrm{Nu}_x/\mathrm{Re}_x^{1/(n+1)}$ are computed in

Table 2. Values of $(-f''(0))$ in the case of Newtonian fluid with $\beta = \varphi = 0$.

Power-law index n	Cortell [47]	Cortell [48]	Present result
n	0.677647	0.677647	0.677649

terms of wall shear stress $(-f''(0))^n$ and local rate of heat transfer $-\theta'(0)$, respectively. To assess the accuracy of the numerical method, we compared the values of the local skin friction $(-f'')$ for $n = 1$ and $\beta = \varphi = 0$ with values obtained in [47,48]. The comparison given in table 2, shows excellent agreement. Numerical calculations were performed in the ranges $0 \leq \beta \leq 0.6, 0 \leq \varphi \leq 0.1, 0.5 \leq n \leq 1.3$ and $0.5 \leq \text{Bi} \leq 40$ with $3.54 \leq \text{Pr}_\infty \leq 7.3$. Figures 2–15 are drawn in order to see the influence of volume fraction of nanoparticles (φ), power-law index (n), viscosity (β) and Biot number (Bi) on the velocity distributions $f'(\eta)$, the temperature distributions $\theta(\eta)$, the local skin friction coefficient $(-f''(0))^n$ and the local Nusselt number $(-\theta'(0))$ for the steady two-dimensional boundary layer flow of Cu–sodium alginate nanofluid along a stretching surface. Figures 2 and 3 show the effects of volume fraction of the nanoparticles φ on the velocity and temperature distributions for both pseudoplastic and dilatant Cu–sodium alginate nanofluids. It is observed that the momentum boundary layer thickness and velocity distributions increase with an increase in volume fraction of the nanoparticles. In addition, the thickness of the thermal boundary layer and the temperature distributions increase with an increase in volume fraction of the nanoparticles. On the other hand, the temperature distributions of the Cu–sodium alginate nanofluid is increased significantly compared to the regular fluid ($\varphi = 0$) for both pseudoplastic and dilatant fluids. Physically, it is interesting to note that the temperature of the Cu–sodium alginate increases significantly because the copper nanoparticles in the fluid have high thermal conductivity. We also notice that the heat transfer rate of the Cu–sodium alginate nanofluid decreases with an increase in volume fraction of the nanoparticles as depicted in figures 12 and 13. These results are similar to those reported by Grosan and Pop [49]. Figures 4–6 show the effects of viscosity (β) and volume fraction of the nanoparticles (φ) on the variable Prandtl number, the velocity and the temperature distributions for both regular fluid ($\varphi = 0$) and Cu–sodium alginate nanofluid. It is observed that the variable Prandtl number, the momentum boundary layer thickness and velocity distributions decrease with

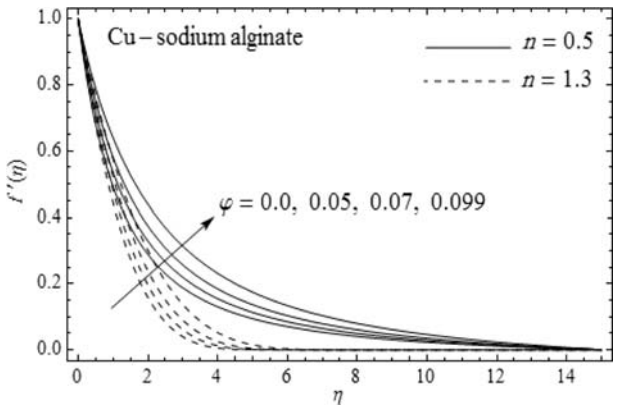

Figure 2. Velocity profiles for various values of φ and n with Bi = 1, $\beta = 0.2$ and $\text{Pr}_\infty = 5$.

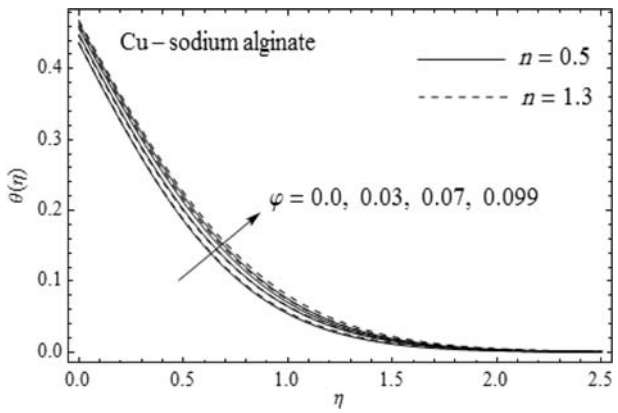

Figure 3. Temperature profiles for various values of φ and n with Bi = 1, $\beta = 0.2$ and $\text{Pr}_\infty = 5$.

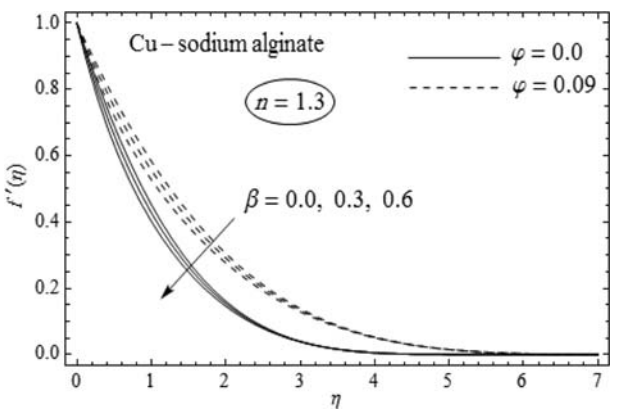

Figure 4. Velocity profiles for different values of β and φ with $n = 1.3$, Bi = 1 and $\text{Pr}_\infty = 5$.

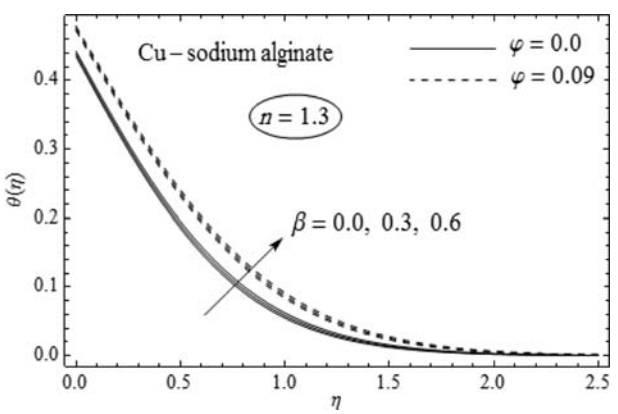

Figure 5. Temperature profiles for different values of β and φ with $n = 1.3$, Bi = 1 and $\text{Pr}_\infty = 5$.

an increase in the viscosity whereas the reverse trend is observed for the thermal boundary layer thickness and the temperature distributions. On the other hand, the velocity and the temperature distributions increase with an increase in the volume fraction of the nanoparticles whereas the reverse trend is observed for the variable Prandtl number. This is because the presence of nanoparticles leads to an increase in viscosity which in turn creates resistance to the fluid motion and enhances the temperature field. This agrees with the physical behaviour that the thermal conductivity increases with increase in the volume fraction of copper and then the thermal boundary layer thickness increases. Furthermore, the thickness of the thermal boundary layer in Cu–sodium alginate nanofluid is greater than that in pure fluid.

Figure 7 shows the effect of Biot number (Bi) on the temperature distributions for both regular fluid ($\varphi = 0$) and Cu–sodium alginate nanofluid. It is observed that the temperature of the fluid and thermal boundary layer thickness increase with an increase in Biot number for both cases. On the other hand, the temperature of the regular fluid is lower than the temperature of the Cu–sodium alginate nanofluid. This may be due to the fact that the thermal conductivity of the base fluid increases with the mixture of the solid nanoparticles. Figures 8–10 show the effects of viscosity (β) on the velocity and the temperature distributions for both pseudoplastic ($n = 0.5$) and dilatant ($n = 1.3$) nanofluids. It is observed that the momentum boundary layer thickness and the velocity distributions decrease with an increase in viscosity whereas the reverse trend is observed for the thermal boundary layer thickness and the temperature distributions. It is noteworthy that by increasing viscosity, the velocity profiles will be lower in dilatant nanofluid, than in pseudoplastic nanofluid. The variations of the local skin friction coefficient and the heat transfer rate with different types of nanoparticles (Cu, Ag, TiO_2 and Al_2O_3) for both cases of pseudoplastic ($n = 0.5$) and dilatant nanofluids ($n = 1.3$) are represented in figures 11–13. It is noticed from figure 11, that the local skin friction coefficient decreases with increasing φ for different

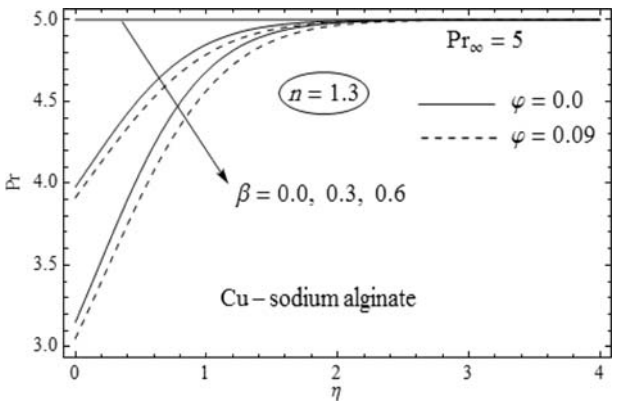

Figure 6. Variation of Prandtl number (Pr) for different values of β and φ with $n = 1.3$ and $\mathrm{Bi} = 1$.

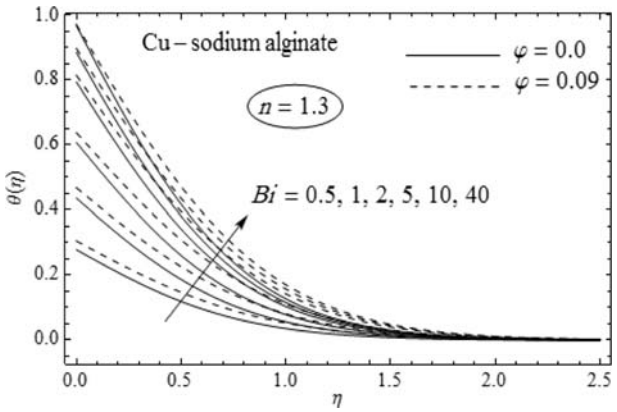

Figure 7. Temperature profiles for different values of Bi and φ with $n = 1.3$, $\beta = 0.2$ and $\mathrm{Pr}_\infty = 5$.

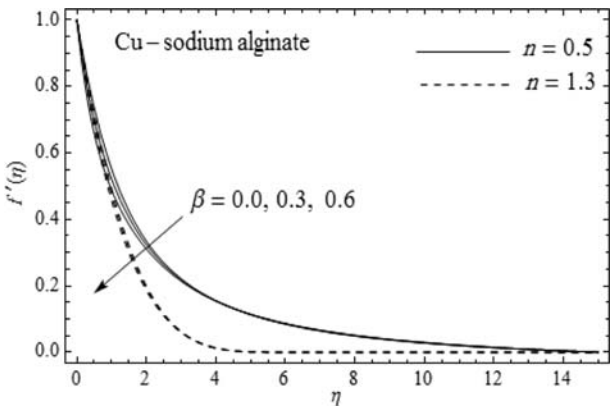

Figure 8. Velocity profiles for different values of β and n with $\varphi = 0.05$, Bi=1 and $\mathrm{Pr}_\infty = 5$.

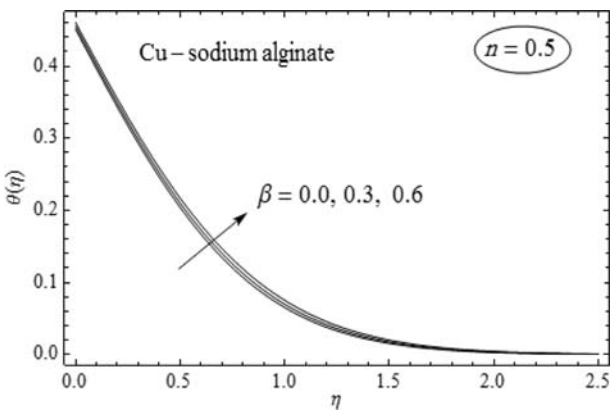

Figure 9. Temperature profiles for different values of β with $n = 0.5$, $\varphi = 0.05$, $\mathrm{Bi} = 1$ and $\mathrm{Pr}_\infty = 5$.

types of nanoparticles. On the other hand, the lowest skin friction coefficient is recorded for the TiO_2– and Al_2O_3–sodium alginate nanofluids compared to other non-Newtonian nanofluids namely, Ag– and Cu–sodium alginate nanofluids. Furthermore, the skin friction coefficient of pseudoplastic nanofluid is greater than that of dilatant nanofluids. It is observed from figures 12 and 13, that the local Nusselt number decreases with increasing φ for different types of nanoparticles. In addition, it is observed that nanoparticles with low thermal conductivity (TiO_2 and Al_2O_3) have better enhancement on heat transfer compared to Ag and Cu. These results are similar to those reported by Lin *et al* [27]. Variations of the local skin friction coefficient and the heat transfer rate for different values of Biot number and viscosity for both pseudoplastic and dilatant nanofluids are plotted in figures 14 and 15. It is found from figures 14 and 15, that the skin friction coefficient and the local Nusselt number increase by increasing the Biot number for Cu–sodium alginate nanofluid. This agrees with the fact that the convective heat transfers from the hot fluid side on the surface to the cold nanofluid side by increasing the Biot number. This serves to increase both the skin friction coefficient and the heat transfer rate for Cu–sodium alginate nanofluid. From figure 14 it is clear that the skin friction coefficient $(-f''(0))^n$ of both pseudoplastic and dilatant nanofluids is greatly increased with the increase in viscosity (β) and this is true for all values of Biot number (Bi). Further, for both pseudoplastic and dilatant nanofluids, the impact of Bi on $(-f''(0))^n$ increases markedly as the viscosity increases (see figure 14).

In addition, it is interesting to note from figure 14 that a single value of $(-f''(0))^n = 0.7920$ for a pseudoplastic and 0.5447 for dilatant nanofluid is obtained for all Bi values when $\beta = 0$ (in the absence of variable viscosity). This is because eqs (28) and (32) are uncoupled when $\beta = 0$, i.e., the solution to the flow field are not affected by the thermal field when temperature-dependent viscosity is not taken into

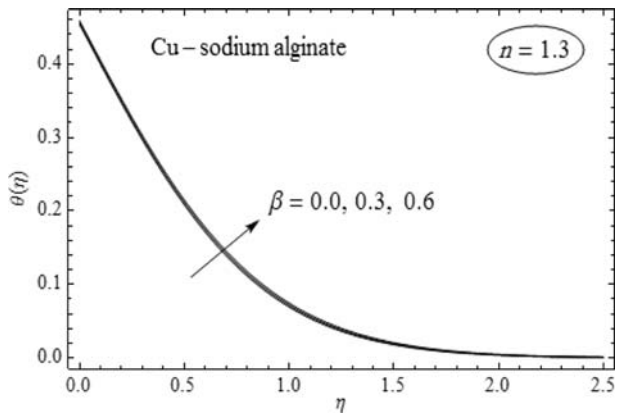

Figure 10. Temperature profiles for different values of β with n =1.3, $\varphi = 0.05$, Bi = 1 and $Pr_\infty = 5$.

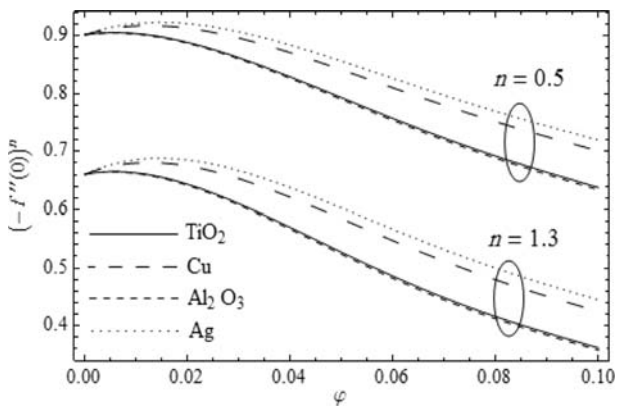

Figure 11. Variation of $(-f''(0))^n$ with φ for different types of nanoparticles and n when Bi = 1, $\beta = 0.2$ and $Pr_\infty = 5$.

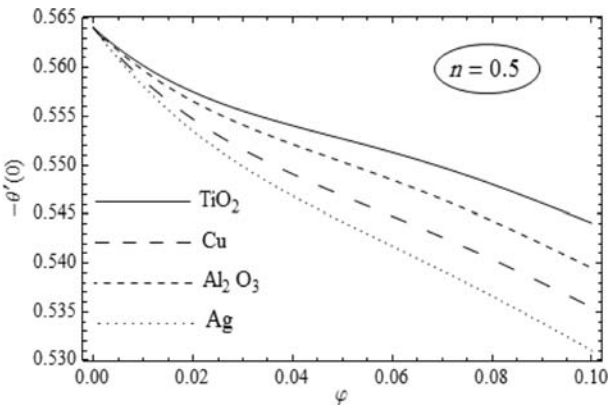

Figure 12. Variation of $-\theta'(0)$ with φ for different types of nanoparticles when Bi = 1, $\beta = 0.2$, $Pr_\infty = 5$ and n = 0.5.

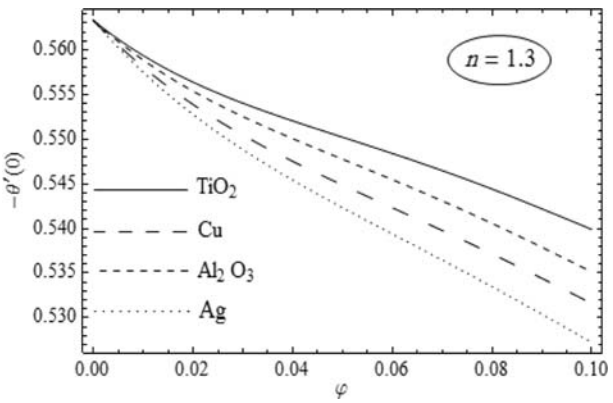

Figure 13. Variation of $-\theta'(0)$ with φ for different types of nanoparticles when Bi = 1, $\beta = 0.2$, $Pr_\infty = 5$ and n = 1.3.

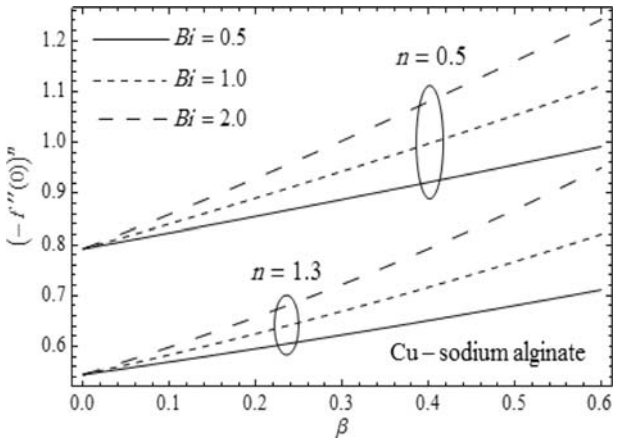

Figure 14. Variation of $(-f''(0))^n$ with β for different values of Bi and n when $\varphi = 0.05$ and $\mathrm{Pr}_\infty = 5$.

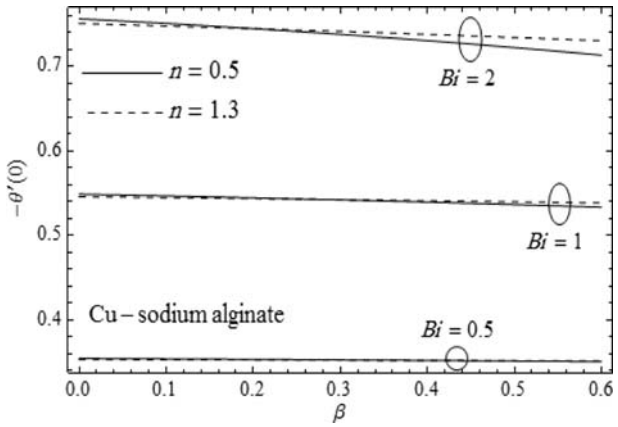

Figure 15. Variation of $-\theta'(0)$ with β for different values of Bi and n when $\varphi = 0.05$ and $\mathrm{Pr}_\infty = 5$.

account. On the other hand, figure 15 shows that the heat transfer rate of both pseudoplastic and dilatant nanofluids is insensitive to change in viscosity for relatively weak (Bi = 0.5, 1) convective heating while it decreases moderately by relatively strong (Bi = 2) convective heating on the back side of the plate. Physically, the viscosity of the base fluid decreases by increasing the temperature which in turn decreases the heat transfer rate. In contrast, an increase in viscosity β leads to an increase in skin friction coefficient of Cu–sodium alginate nanofluid. It is further noticed from figure 15, that for relatively high values of Biot number, the heat transfer rate of the pseudoplastic nanofluid is higher than that of the dilatant nanofluids up to $\beta = 0.2$ whereas the situation is completely reversed for $\beta > 0.2$ but this situation is insignificant for relatively small values of Biot number (Bi = 0.5, 1). On the other hand, Biot number has a significant effect on the skin friction coefficient if viscosity is increased.

5. Conclusions

In the present paper, Lie symmetry group transformations are applied to find similarity solutions of boundary layer flow and heat transfer over a non-linearly stretching surface embedded in non-Newtonian nanofluids. The effects of convective boundary conditions, temperature-dependent fluid viscosity and the power-law index have been investigated. The results are discussed through graphs. It is observed that the heat transfer rate decreases with an increase in nanoparticle volume fraction for different types of non-Newtonian nanofluids. The nanoparticles with low thermal conductivity, alumina (Al_2O_3) and titania (TiO_2), can enhance the heat transfer better than copper (Cu) and silver (Ag). The skin friction coefficients for both pseudoplastic and dilatant nanofluids increase greatly with an increase in viscosity β. It is noticed that the heat transfer rates for both pseudoplastic and dilatant nanofluids are insensitive to change in viscosity β for lower values of Biot number (Bi = 0.5, 1) while it increases moderately with higher values of Biot number (Bi = 2). The skin friction coefficient and the rate of heat transfer increase with an increase in Biot number (Bi) for Cu–sodium alginate nanofluid. The velocity and temperature distributions increase with an increase in volume fraction whereas the opposite effects occur with the variable Prandtl number. It is further noticed that the variable Prandtl number and velocity distributions decrease with an increase in viscosity β whereas the reverse trend is observed for temperature distributions.

Acknowledgements

The authors are very thankful to the reviewers for their encouraging comments and constructive suggestions to improve the presentation of this manuscript.

References

[1] L J Crane, *Z. Angew. Math. Phys.* **21**, 645 (1970)
[2] P S Gupta and A S Gupta, *Can. J. Chem. Eng.* **55**, 744 (1977)
[3] L J Grubka and K M Bobba, *ASME J. Heat Transfer* **107**, 248 (1985)
[4] N Bachok, A Ishak and R Nazar, *Meccanica* **46**, 935 (2011)
[5] L Zheng, L Wang and X Zhang, *Commun. Nonlinear Sci. Numer. Simul.* **16**, 731 (2011)
[6] E H Aly and K Vajravelu, *Appl. Math. Comput.* **232**, 191 (2014)
[7] H I Andersson, K H Bech and B S Dandapat, *Int. J. Non-Linear Mech.* **27**, 929 (1992)
[8] R Cortell, *Appl. Math. Comput.* **168**, 557 (2005)
[9] S-J Liao, *J. Fluid Mech.* **488**, 189 (2005)

[10] K V Prasad, S R Santhi and P S Datti, *Appl. Math.* **3**, 425 (2012)
[11] M Madhu and N Kishan, *J. Egypt. Math. Soc.* **24**, 458 (2016)
[12] S U S Choi, *ASME Fluids Eng. Div.* **231**, 99 (1995)
[13] N Putra, W Roetzel and D K Das, *Heat Mass Transfer* **39**, 775 (2003)
[14] J A Eastman, S U S Choi, S Li, W Yu and L J Thompson, *Appl. Phys. Lett.* **78**, 718 (2001)
[15] J Buongiorno, *J. Heat Transf. Trans. ASME* **128**, 240 (2006)
[16] M Abd El-Aziz, *Int. J. Mod. Phys. C* **24**, 1 (2013)
[17] A A Afify and M A A Bazid, *J. Comput. Theor. Nanosci.* **11**, 1844 (2014)
[18] K S Hwang, S P Jang and S U S Choi, *Int. J. Heat Mass Transfer* **52**, 193 (2009)
[19] K Das, *Microfluid Nanofluid* **15**, 267 (2013)
[20] P Loganathan and C Vimala, *Indian J. Phys.* **88**, 855 (2014)
[21] R Kamali and A R Binesh, *Int. Commun. Heat Mass Transfer* **37**, 1153 (2010)
[22] M Hojjat, S G Etemad, R Bagheri and J Thibault, *Int. Commun. Heat Mass Transfer* **38**, 144 (2011)
[23] S S Pawar and V K Sunnapwa, *Exp. Therm. Fluid Sci.* **44**, 792 (2013)
[24] M Hatami and D D Ganji, *J. Mol. Liq.* **188**, 155 (2013)
[25] M Hatami and D D Ganji, *Case Studies Therm. Eng.* **2**, 14 (2014)
[26] A Esmaeilnejad, H Aminfar and M S Neistanak, *Int. J. Therm. Sci.* **75**, 76 (2014)
[27] Y Lin, L Zheng and X Zhang, *Int. J. Heat Mass Transfer* **77**, 708 (2014)
[28] O D Makinde and A Aziz, *Int. J. Therm. Sci.* **53**, 2477 (2011)
[29] S Nadeem, R Mehmood and N S Akbar, *Int. J. Therm. Sci.* **78**, 90 (2014)
[30] E Abu-Nada, *Int. J. Heat Fluid Flow* **30**, 679 (2009)
[31] K Vajravelu and K V Prasad, *J. Mech.* **28**, 579 (2012)
[32] A A Afify and M A A Bazid, *J. Comput. Theor. Nanosci.* **11**, 2440 (2014)
[33] H F Oztop and E Abu-Nada, *Int. J. Heat Fluid Flow* **29**, 1326 (2008)
[34] X Wang, X Xu and S U S Choi, *J. Thermophys. Heat Transfer* **13**, 474 (1999)
[35] J Maxwell, *A treatise on electricity and magnetism* 2nd edn (Oxford University Press, Cambridge, UK, 1904)
[36] Y Khana, Q Wua, N Faraz and A Yildirim, *Comput. Math. Appl.* **61**, 3391 (2011)
[37] M S Abel, P S Datti and N Mahesha, *Int. J. Heat Mass Transfer* **52**, 2902 (2009)
[38] M Jalil and S Asghar, *Int. J. Nonlinear Mech.* **48**, 65 (2013)
[39] M B Akgül and M Pakdemi, *Sci. Iran.* **19**, 1534 (2012)
[40] T Tapanidis, Gr Tsagas and H P Mazumdar, *Nonlinear Funct. Anal. Appl.* **8**, 345 (2003)
[41] A A Afify and N S Elgazery, *Nonlinear Anal. Model. Control* **17**, 1 (2012)
[42] A G Hansen, *Similarity analysis of boundary layer problems in engineering* (Prentice Hall, Englewood Cliffs, NJ, USA, 1964)
[43] A Pantokratoras, *Int. J. Heat Mass Transfer* **45**, 963 (2002)
[44] A Pantokratoras, *Int. J. Eng. Sci.* **42**, 1891 (2004)
[45] M M Rahman, M A Rahman, M A Samad and M S Alam, *Int. J. Thermophys.* **30**, 1649 (2009)
[46] H I Andersson and V Kumaran, *Int. J. Non-Linear Mech.* **41**, 1228 (2006)
[47] R Cortell, *J. Mater. Process. Technol.* **203**, 76 (2008)
[48] R Cortell, *Appl. Math. Comput.* **217**, 7564 (2011)
[49] T Grosan and I Pop, *J. Heat Transfer* **133**, 054503 (2011)